

Three dimensional passive sensing, imaging, and visualization

Ju-Seog Jang* and Bahram Javidi*

University of Connecticut, Electrical and Computer Engineering Department, 371 Fairfield Road,
U-2157, Storrs, CT 06269-2157

Email: bahram@engr.uconn.edu

ABSTRACT

In this paper, we present an overview of 3-D image sensing, formation, and visualization using integral imaging (II). As 2-D sensors and 2D display panel technologies advance rapidly, real-time 3D sensing and imaging have shown great promise for 3-D sensing, 3D TV and 3D visualization.

Keywords: Integral imaging; three-dimensional image display; image display; image resolution

1. INTRODUCTION

Display technologies are well developed, and so far high-resolution color images are used in computer monitors, TV, etc. However, these images are mostly two-dimensional (2-D) images and do not exhibit depth. Display of 3-D images that can present high quality real 3-D objects is still elusive. There has been much effort to realize 3-D display.¹⁻⁴ So far the most successful 3-D display technique is a stereoscopic method, in which two 2-D images with binocular parallax (i.e., left-eye image and right-eye image) are presented to the observers' left and right eyes, respectively, to evoke 3-D perception. Thus supplementary glasses are usually required to suppress the other image at each eye. In stereoscopic techniques, however, observers see usually a fixed viewpoint, and may experience visual fatigue because of convergence-accommodation conflict, which is a serious disadvantage.⁴

To remove convergence-accommodation conflict, true 3-D images with full parallax and continuous viewing points should be formed in space. Holography is the most successful technique to form 3-D images in space. However, coherent light is usually necessary in recording holograms. Speckle is also a problem. Recently, another 3-D image formation technique called integral imaging (II) is studied actively based on ray optics. In II, 3-D images are formed by integrating the rays coming from 2-D elemental images using a lenslet (or pinhole) array. II was first proposed by Lippmann in 1908 under the name of integral photography.⁵⁻⁸ As 2-D display panel technology advances rapidly, real-time integral photography, or II, using display panels and light sensitive electronic devices has shown great promise for 3-D TV and visualization.^{9,10} In this paper, we present an overview of 3-D image sensing, formation, and visualization using integral imaging (II).^{4,5,8}

2. INTEGRAL IMAGING SYSTEM

II can be easily understood if we consider a hypothetical ideal 3-D image recording and display device as depicted in Fig. 1(a). If information on directions and intensities of optical rays originated from a 3-D object is recorded in the detector device, a 3-D image of the object can be reconstructed by generating the rays with the same directions and intensities from the device. If the directions of reconstructing rays are exactly opposite to those of recording rays, a pseudoscopic (depth-reversed) real image will be formed. If the directions of reconstructing rays are exactly the same as those of recording rays, an orthoscopic virtual image will be formed. The hologram is a good example. As depicted in Fig. 1(b), the information on the object rays is stored in a photographic plate as an interference pattern (that is, gratings) of the object rays and a reference beam in the hologram. When the reference beam used to record the hologram is used as a read-out beam, an orthoscopic virtual image will be formed. When a conjugate reference beam illuminates the hologram, the rays with a similar intensity distribution but with opposite directions are generated from the hologram to form a pseudoscopic real image.

* email: bahram@engr.uconn.edu; phone 1 860 486-2867; fax 1 860 486-6339

One important advantage of II is that it can operate under incoherent illumination. To record the ray information in a 2-D light-sensitive device such as a CCD, either a pinhole array or a lenslet array is used as depicted in Fig. 1(c) and 1(d). Each pinhole (or lenslet) samples the ray information at its location. The ray information sampled by a pinhole (or lenslet) and detected by detector array looks like a small image projection of the object. So it is often referred to as an elemental image. To reconstruct a 3-D image from the recorded elemental images, a display panel, such as a liquid crystal display (LCD), for the elemental image display and a pinhole (or lenslet array) for selecting proper ray directions are needed. Because the light efficiency of the pinhole array is very low, a lenslet array is usually used in actual pickup and display processes. The reconstructed image depicted in Fig. 1(d) is a pseudoscopic real image. This pseudoscopic image can be converted to an orthoscopic virtual image as depicted in Fig. 1(e) by rotating every elemental image around its own center optic axis by 180 degrees.¹⁰ It is also possible to display an orthoscopic real image by introducing an additional imaging lens in front of the pickup lenslet array.

Computational II is often used, in which a 3-D image is reconstructed in a computer using elemental images picked up by a CCD rather than optical reconstruction using a LCD and lenslet array.¹¹ In computational II, a hypothetical pinhole array is used for simplicity to simulate the display process depicted in Fig. 1(d) according to geometrical optics. Similarly, the pickup process can be simulated by a computer, and computer-generated integral images can be displayed by a LCD.¹²

Compared with stereoscopic techniques, however, II does not produce 3-D images with competitive resolution, viewing angle, and longitudinal depth. There were many studies to overcome the limited 3-D image quality in II.

3. IMAGE RESOLUTION OF INTEGRAL IMAGING AND IMPROVEMENTS USING TIME MULTIPLEXING

As in conventional optical imaging systems, the image resolution in II is determined by many system parameters, for example, the lenslet size, the resolution of the CCD and the display device, lenslet aberrations, misalignment, etc. In II, there is an additional factor that limits the 3-D image resolution: It is the pitch of the lenslet arrays, which determines the spatial sampling rate of the ray information in the spatial dimension. From the Nyquist sampling theorem, the upper limit of the viewing resolution in a lateral dimension is given by $\beta_{\text{nyq}} \approx L_o / 2p$ in cycles per radian (cpr), where L_o is the distance between the observation point and the display lenslet array and p is the pitch of the pinhole (lenslet) array.¹³ However, if we reduce p (i.e., the size of lenslets), diffraction of the lenslets limits the resolution even though the resolution of the detector and the display is sufficiently large. Many authors have studied an optimal lenslet size, which is around 1 or 2 mm in reasonable viewing circumstances.¹⁴ For example, we may have $p = 1$ mm and $L_o = 1$ m (i.e., $\beta_{\text{nyq}} = 500$ cpr). This means that we cannot discern images whose size is less than about 2 mm from distance of 1 m. Such low resolution limits the usefulness of II in practical applications.

To increase the spatial sampling rate, a time-multiplexing technique has been proposed, in which the positions of the lenslet arrays for both pickup and display are rapidly vibrated synchronously in the lateral directions within the retention time of the after-image (or, faster than the flicker fusion frequency) of the human eye.¹⁵ The vibration (or movement) range needs not be larger than one lenslet pitch in both lattice directions, because the lenslet arrays are periodic. The elemental image detection device (CCD array) and the image display device (LCD) are stationary. Because the pickup lenslet array and the display lenslet array vibrate synchronously and human eyes have the effect of an averaging detector, observers see a stationary reconstructed image with improved viewing resolution for a stationary object.

When the lenslets are packed in a square lattice with a pitch of p , 2-D motions are necessary to increase the spatial sampling rate along mutually orthogonal two lattice directions in general. Because the lenslet arrays have a periodic structure, however, even if the lenslet arrays move only along the x axis with a velocity of V , we can increase the sampling rate along the two lattice directions (x' and y' directions) by tilting the lenslet arrays by θ where θ is the angle between x and x' . This circumstance is depicted in Fig. 2(a). In this case, the velocity component of the lenslet array in x' direction becomes $V \cos \theta \equiv V_{x'}$, while that in y' direction $V \sin \theta \equiv V_{y'}$. As lenslets move, elemental images also move. Moving (i.e., time-varying) elemental images are detected (or sampled) by the 2-D image sensor and then displayed in the display panel (or LCD). The time-sampled elemental images should be integrated in time domain in the observer's eyes without flickering. Because the lenslet array has a periodic structure, the elemental image pattern

repeats in time domain as the pickup lenslet array moves. For stationary objects, therefore, $V_{x'}$ and $V_{y'}$ should satisfy the following conditions: $V_{x'} = V \cos \theta > pS$ and $V_{y'} = V \sin \theta > pS$, where S is the flicker fusion frequency of the human eye. When the objects to be imaged move with maximum velocity of V_{\max} , the velocity of the lenslet arrays should be increased accordingly for time-domain integration without flickering in the eye. For a stationary object, because S is approximately 50 Hz for human eyes, we get $V > 70$ [mm/sec] when $\theta = 45$ degrees and $p = 1$ mm. In conventional TV and video systems, the frame rate is fixed typically at 60 Hz (or, two 30-Hz frames are interlaced). So, there exists a limit to display a fast moving object, because the time-domain resolution is also limited by the Nyquist sampling rate in time domain. In the proposed time multiplexing technique, the increase of the spatial sampling rate of ray information by lenslets is achieved in time dimension. Therefore, the frame rate of 2-D image sensor and the display panel should be increased by a factor of $\max(p/V_{x'}, p/V_{y'})$ to support the lenslet movement. This is the price that we have to pay for the resolution improvement.

In fact, the movement of the lenslet arrays need not be linear. For practical applications, a circular motion of the lenslets could be used as depicted in Fig. 2(b). In this case, the radius of the circular motion should be larger than one half pitch of the lenslets. To maintain strict synchronization between the two lenslets for pickup and display in 3-D TV systems, a clock signal will be necessary in controlling their circular motions.

Figure 3(a) depicts a typical II system, and Fig. 3(b) shows the system setup to demonstrate the effect of lenslet movement. Assuming that the resolutions of both the detector and the display devices in Fig. 3(a) (See the dashed box) are sufficiently large, we use a pair of lenslet arrays as shown in Fig. 3(b). The first lenslet array is used to obtain multiple elemental images and the second lenslet array is used to reconstruct the 3D image. The gap between the two lenslet arrays was adjusted to minimize the focusing error.

The object used for 3D imaging is composed of a die and a plastic button with a footprint figure as shown in Fig. 4. The side length of the die is 1.5 cm and the diameter of the button is 1 cm. The distance between the die surface with four dots and the button surface with the footprint figure is about 3 cm. The lenslet arrays we used have 53×53 identical lenslets. Each lenslet element is square-shaped and has a uniform base size of $1.09 \text{ mm} \times 1.09 \text{ mm}$, with less than $7.6 \mu\text{m}$ separating the lenslet elements. The focal length of the lenslets is approximately 3 mm. The tilting angle of the lenslet arrays θ was set to 30 degrees. The distance between the pickup lenslet array and the front surface of the die is roughly 7 cm. The real pseudoscopic image is detected by a CCD with a standard camera lens and a built-in iris. The distance between the real image and the display lenslet array is roughly 10 cm, and that between the real image and the camera lens is approximately 50 cm.

The reconstructed image is shown in Fig. 5(a). We set the pupil diameter of the camera iris to approximately 10 mm, in order to make the condition of the camera lens and the CCD be similar to the human eye whose pupil diameter is about 3 mm in an ordinary environment. The die dots, which are larger than the size of each lenslet element, are distinguishable. However, the toes in the footprint figure, which are similar to or slightly smaller than the size of each lenslet element, are not clear. When we set in motion the two lenslet arrays for both pickup and display synchronously in the horizontal direction, the resolution is improved and the toes are clear as shown in Fig. 5(b). To show the 3D nature of the reconstructed image, we changed the position (and accordingly the viewing direction) of the CCD camera and repeated the experiment. The reconstructed 3D images captured by the CCD camera are shown in Fig. 5(c) and 5(d). It is evident that if the viewing position is changed, one dot in the left surface of the die appears.

4. VIEWING ANGLE AND TIME MULTIPLEXING

As we can see in Fig. 5(c) and (d), multiple 3-D images are reconstructed in the display process, if optical barriers that isolate elemental images are not used. This is because elemental images are also displayed through neighboring lenslets, which results in higher order reconstructed images. The viewing angle can be defined as a range of diverging angle over which one can see only the zero-order reconstructed 3-D image. From Fig. 6, the viewing angle ψ is defined mathematically as $\psi = \arctan(p/2g)$ where g is the gap between the lenslet array and the display panel (or CCD). For a given lenslet size and gap g (or focal length), ψ increases as p increases. [See Fig. 6(b).] However, as p increases, the sampling resolution β_{nyq} decreases. The moving lenslet technique can increase the ray sampling rate

by time multiplexing. Therefore, we can increase the separation of lenslet elements to improve ψ . In other words, for a given size of lenslets, the pitch of the lenslet arrays is increased. Consequently, the fill-factor of the lenslet array reduces assuming that we are using an optimal lenslet size. When the lenslet size is too large, 3-D images with large image depth cannot be integrated because of the short depth of focus for each lenslet. When the lenslet size is too small, diffraction also influences the image quality. The resolution obtained using the time-multiplexing technique with low fill factor lenslet arrays is higher than that obtained using lenslet arrays with a high fill factor without time-multiplexing technique.¹⁶

To demonstrate the effect of viewing angle improvement, we repeated the same experiment using the lenslet arrays with an amplitude mask which blocks every other lenslet along both lattice directions. So, the lenslet pitch is increased by a factor of two. Without using the time-multiplexing technique, the quality of the reconstructed 3-D image is given in Fig. 7(a) which is poor compared with that given in Fig. 5(a), because of the increased lenslet pitch. However, when the time-multiplexing technique is used, the image quality is improved as shown in Fig. 7(b). Because the fill factor of the lenslet arrays is low (due to the masks), the light loss is increased and the reconstructed image becomes dark. However, the viewing resolution of the image in Fig. 7(b) is good enough to clearly distinguish the toes. When we changed the position (and accordingly the viewing angle) of the CCD camera as before, multiple images were not observed as shown in Fig. 7(c) and 7(d). This is because the viewing angle has been enhanced ($\psi \approx 40$ degrees) due to the low lenslet pitch.

5. IMAGE RESOLUTION AND LONGITUDINAL IMAGE DEPTH

In II, one cannot integrate rays to produce 3-D images with arbitrarily large depth of focus in II.¹⁷ Suppose that point images are to be displayed in the real image space ($z > 0$) by use of an ideal diffraction-limited II system, as depicted in Fig. 8. Suppose also that the lenslet array is composed of square-shaped lenslets. The focal length and the side length of each lenslet are denoted by f_i and d_i , respectively. For simplicity, we assume that the display panel has sufficient resolution. Then, the elemental images are represented by properly positioned light emitting pixels in the display panel. Let us consider that the lenslet image plane is located at the integral image plane, as depicted in Fig. 8(a). If the distance between the lenslet array and the lenslet image plane is L_i , the gap distance g should be $g = L_i f_i / (L_i - f_i)$ according to the Gauss lens law. The minimum spot size of the integral point image we can get at the lenslet image plane is given by $2\lambda L_i / d_i \equiv s$ from the Fraunhofer diffraction of the square-aperture lenslet. Here, we will not consider the limit of spatial ray sampling effect in the lenslet array, assuming that the time-multiplexing technique is used. Then, the maximum resolution R , in lines/mm, is given by $R = 1/s = d_i / 2\lambda L_i$. However, the image resolution cannot be maintained when a 3-D image with large depth is produced. This is because the spot size of the integral point image increases (or the point image blurs) quickly as the distance between the integral image plane and the lenslet image plane (denoted by Δz) increases, as shown in Fig. 8(b). We define the depth limit of 3-D integral images as the depth-of-focus of the lenslet based on the widely used Rayleigh limit, denoted by Δz_f . Assuming that $d_i / 2L_i \ll 1$, we get $\Delta z_f = 2\lambda L_i^2 / d_i^2$. Integral images can be produced on both sides of the lenslet image plane if $\Delta z_f < L_i$, as shown in Fig 8(a). Therefore, we define the maximum depth limit of 3-D images that can be displayed in II as $D = 2\Delta z_f = 4\lambda L_i^2 / d_i^2$. As a result, regardless of lenslet size and focal length, we can see that the product of depth-of-focus and resolution square is given by

$$DR^2 = 1/\lambda.$$

For example, if $d_i = 1$ mm, $\lambda = 0.6$ μm , and $L_i = 100$ mm, we get $R = 8.3$ lines/mm, or the spot size of the point integral image is 120 μm . In this case, the image depth is $D = 24$ mm, which is too small to display deep 3-D images. To display 3-D integral images with large depth of focus, we need to increase L_i / d_i , which sacrifices the resolution according to the DR^2 limit.

The above argument is similarly applied to the case when a virtual image is displayed as depicted in Fig 8(c) and (d). In this case, $g = L_i f_i / (L_i + f_i)$ from the Gauss lens law, and the integral image plane and the lenslet image plane for the virtual image are located at $z < 0$.

6. INTEGRAL IMAGING WITH A NON-UNIFORM LENSLET ARRAY

A possible solution to increase the 3-D image depth of focus without sacrificing the spatial resolution is to use an array of lenslets with varying focal lengths and aperture sizes.¹⁸ Suppose that we are using a lenslet array, which is composed of M different sets of lenslets with varying focal lengths and aperture sizes. To increase depth of focus, we choose every lenslet set to produce the same spot size s and the same depth of focus D but at different lenslet image planes, L_1, L_2, \dots, L_M , as shown in Fig 9(a). The i th lenslet in each set contributes to formation of a sharply focused part of a 3-D image in the region $L_i - D/2 < z < L_i + D/2$, where D is depth of focus. To meet these conditions, the distance between the LIP and the lenslet array, the side length, and the focal length of the $(i+1)$ th lenslet should become, respectively,

$$\begin{aligned} L_{i+1} &= L_i + D = L_i + 4\lambda L_i^2 / d_i^2, \\ d_{i+1} &= d_i + 4\lambda L_i / d_i = d_i + 2s, \\ f_{i+1} &= g L_{i+1} / (g + L_{i+1}). \end{aligned}$$

L_i and d_i increase linearly as index i increases, but f_i does not. Practically, it is difficult to obtain a lens with a f number (defined by the ratio of lens size to focal length) close to 1. So, M is limited for given d_1, L_1 , and f_1 . The total image depth becomes MD , while the maximum resolution that can be achieved is maintained at $R = 1/s = d_i / 2\lambda L_i$. Thus, the product of depth-of-focus and resolution square is increased by a factor of M .

An example of the lenslet parameter calculation is illustrated. In this example, $s = 240 \mu\text{m}$ (or $R = 4.17$ lines/mm), $D = 96$ mm, $g = 5.26$ mm, and $M = 9$. So, the total 3-D image depth MD becomes 864 mm. A simple arrangement of these 9 kinds of lenslets in a group is illustrated in Fig. 9(b), although there are many other possible arrangements. The viewing angle is now given by $\psi = 2\arctan(p_e / 2g)$ where $p_e = d_M$ is the pitch of the lenslets. The pitches of the lenslet group in the vertical and horizontal directions are the same in this example, and are denoted by p_g .

The area between lenslets should be blocked by use of a proper amplitude mask. If the blocking portion is not wide, we can compensate the light loss by increasing the illumination intensity. However, other systems (and lenslet array) designs that can avoid or alleviate the blocking area problem may be necessary for a more light-efficient system.

In our proposed method, the elemental images of an object that will be displayed are obtained by computer synthesis as follows. First, we assume that the 3-D image surface is positioned in the same way observers will watch when the elemental images are displayed later, as depicted in Fig. 10. The pitch of the hypothetical pinhole array should be equal to p_e . The light intensity distribution of the corresponding pickup surface $S_p(x_i, y_i, z = -g)$ becomes, for

$L_i - D/2 < z < L_i + D/2$ (i.e., for the i th image slice),

$S_p(x_i, y_i, -g) = (C / d_i^2) \cdot S_o(zx_i / g, zy_i / g, z)$ where C is a constant, and $S_o(\cdot)$ is the reconstructed 3-D object displayed at L_i plane. The factor C / d_i^2 is introduced to compensate the different light efficiencies caused by different lenslet sizes.

In our approach, the i th image slice is produced by only the sets of i th lenslets in all the lenslet groups. Therefore, the pitch that determines the ray sampling effect is the group pitch p_g . When M is power of two, $p_g = \sqrt{M} p_e$. The maximal resolution limit of the i th reconstructed image slice is determined by the Nyquist ray sampling rate, which is proportional to $1/p_g$. If M is increased to improve the image depth, the resolution is decreased because of the

reduced ray sampling rate. To overcome the sampling resolution limit, we can use the time-multiplexing technique described earlier.

7. CONCLUSION

In conclusion, we have shown that a time-multiplexing technique can be used in II to improve both resolution and viewing angle of 3-D images. We also discussed the relation between the resolution and the depth of focus of 3-D images. In conventional II systems, the resolution can be improved by sacrificing the image depth or vice versa because the product of depth-of-focus and resolution square is limited by the inverse of the illumination wave length. When a proper non-uniform lenslet array (with lenslets having varying focal length and lenslet size) is used with the time-multiplexing technique, it is possible to improve both the resolution and the depth of focus of 3-D images. To avoid mechanical movements in our method, an electronically synthesized lenslet array can be used.¹⁹

ACKNOWLEDGMENT

*This paper is dedicated to the memory of Dr. Ju-Seog Jang (1961-2004).

REFERENCES

1. S. A. Benton, ed., *Selected Papers on Three-Dimensional Displays* (SPIE Optical Engineering Press, Bellingham, WA, 2001).
2. N. A. Valyus, *Stereoscopy* (Focal Press, London, 1966).
3. T. Okoshi, *Three-Dimensional Imaging Techniques* (Academic, New York, 1971).
4. B. Javidi and F. Okano, eds., *Three Dimensional Television, Video, and Display Technologies* (Springer, Berlin, 2002).
5. G. Lippmann, "La photographie integrale," *Comptes-Rendus Academie des Sciences* **146**, 446-451 (1908).
6. M. G. Lippmann, "Epreuves reversibles donnant la sensation du relief," *J. Phys. (Paris)* **7**, 821-825 (1908).
7. H. E. Ives, "Optical properties of a Lippmann lenticulated sheet," *J. Opt. Soc. Am.* **21**, 171-176 (1931).
8. J. S. Jang and B. Javidi, "Three-dimensional TV and Display with Large Depth of Focus and Improved Resolution," *Optics and Photonics News Magazine*, pp. 36-43, April 2004.
9. T. Motoki, H. Isono, and I. Yuyama, "Present status of three-dimensional television research," *Proc. IEEE* **83**, 1009-1021 (1995).
10. F. Okano, H. Hoshino, J. Arai, and I. Yuyama, "Real-time pickup method for a three-dimensional image based on integral photography," *Appl. Opt.* **36**, 1598-1603 (1997).
11. H. Arimoto, and B. Javidi, "Integral three-dimensional imaging with digital reconstruction," *Opt. Lett.* **26**, 157-159 (2001).
12. B. Lee, S. -W. Min, and B. Javidi, "Theoretical analysis for three-dimensional integral imaging systems with double devices," *Appl. Opt.* **41**, 4856-4865 (2002).
13. H. Hoshino, F. Okano, H. Isono, and I. Yuyama, "Analysis of resolution limitation of integral photography," *J. Opt. Soc. Am. A* **15**, 2059-2065 (1998).
14. C. B. Burckhardt, "Optimum parameters and resolution limitation of integral photography," *J. Opt. Soc. Am.* **58**, 71-76 (1968).
15. J.-S. Jang and B. Javidi, "Improved viewing resolution of three-dimensional integral imaging with nonstationary micro-optics," *Opt. Lett.* **27**, 324-326 (2002).
16. J.-S. Jang and B. Javidi, "Improvement of viewing angle in integral imaging by use of moving lenslet arrays with low fill factor," *Appl. Opt.* **42**, 1996-2002 (2003).
17. J.-S. Jang, F. Jin, and B. Javidi, "Three-dimensional integral imaging with large depth of focus using real and virtual image fields," *Opt. Lett.* **28**, 1421-1423 (2003).
18. J.-S. Jang and B. Javidi, "Large depth-of-focus time-multiplexed three-dimensional integral imaging using lenslets with non-uniform focal lengths and aperture sizes," *Opt. Lett.* **28**, 1924-1926 (2003).
19. J.-S. Jang and B. Javidi, "Three-dimensional integral imaging with electronically-synthesized lenslet arrays," *Opt. Lett.* **27**, 1767-1769 (2002).

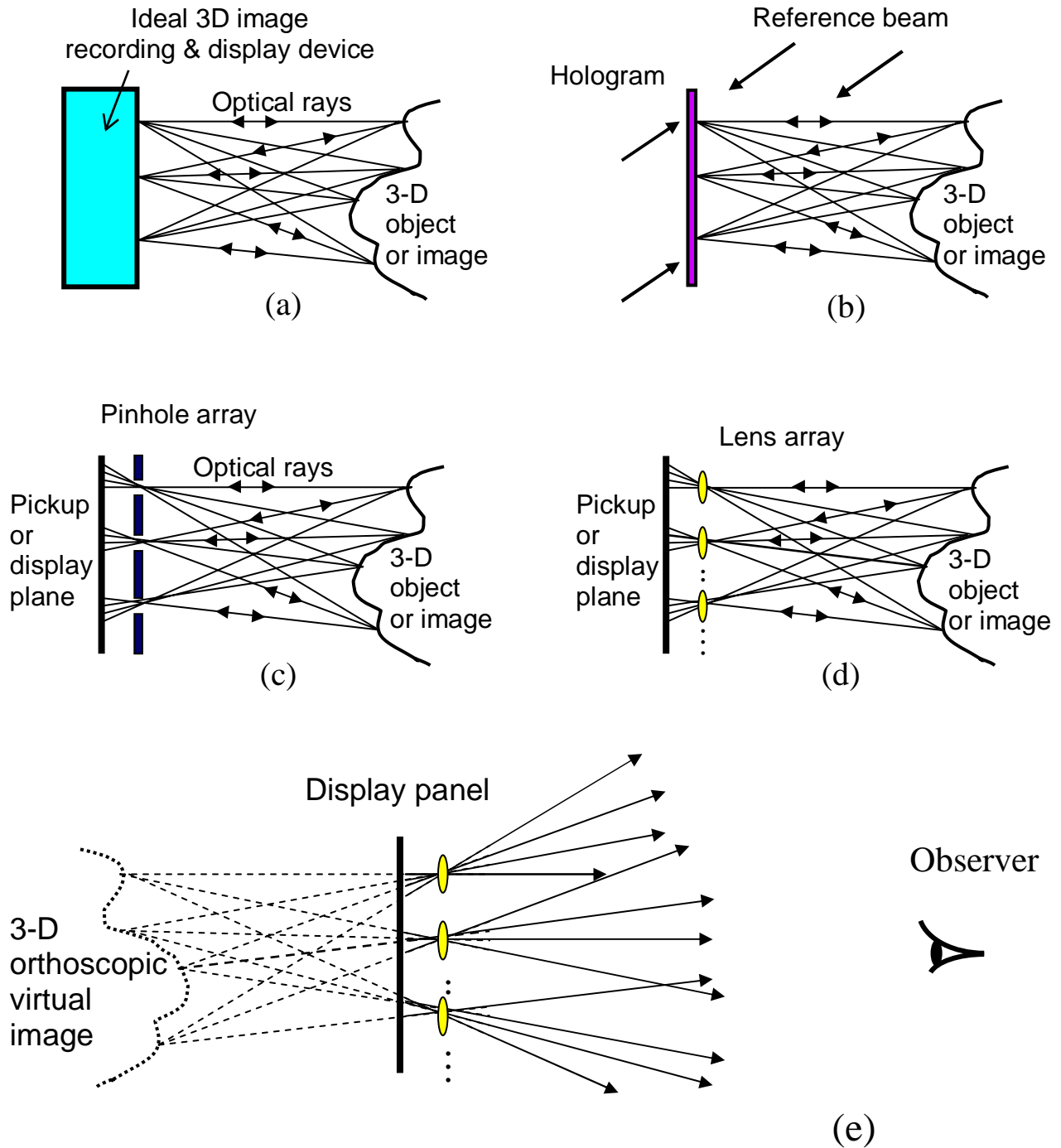


Fig. 1. 3-D image recording and display. (a) Using a hypothetical device. (b) Using a hologram. (c) Using a pinhole array. (d) Using a lenslet array. (e) Display of an orthoscopic virtual image.

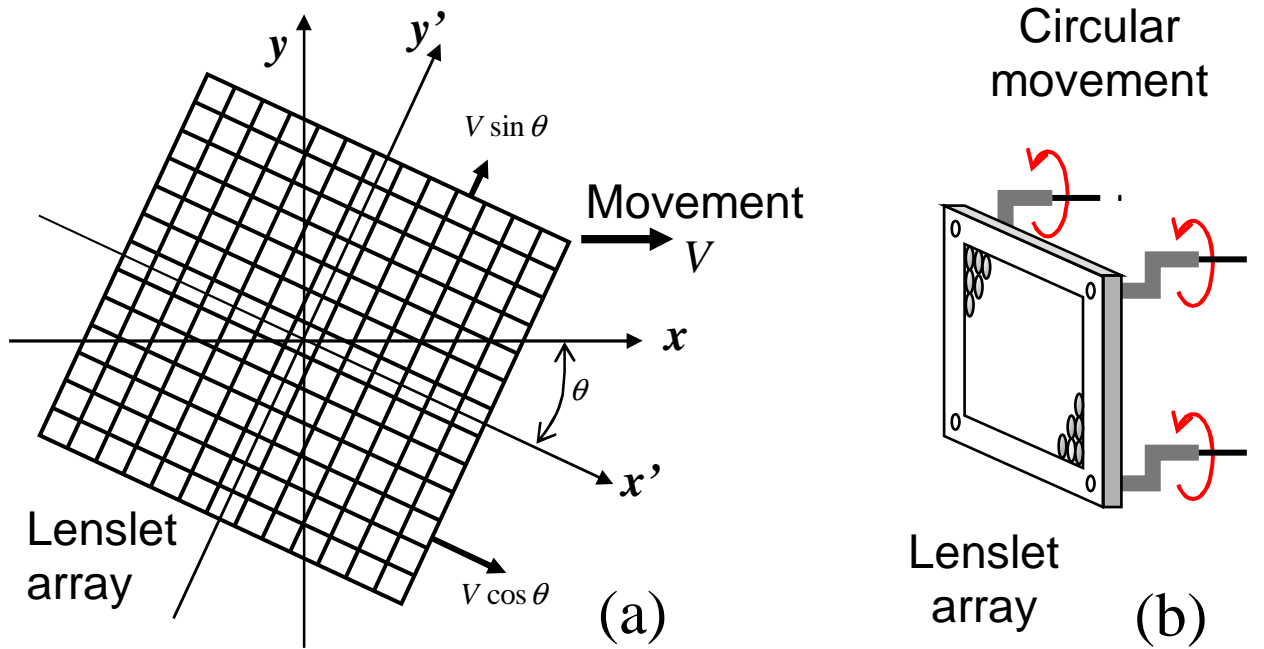


Fig. 2. Movement of lenslet array. (a) A linear movement. (b) A circular movement.

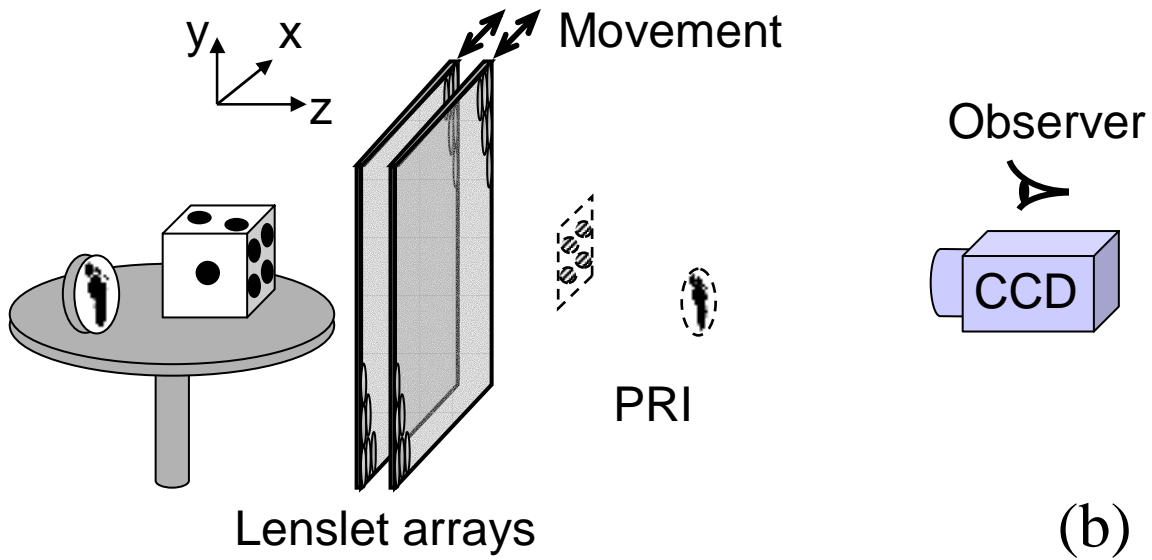
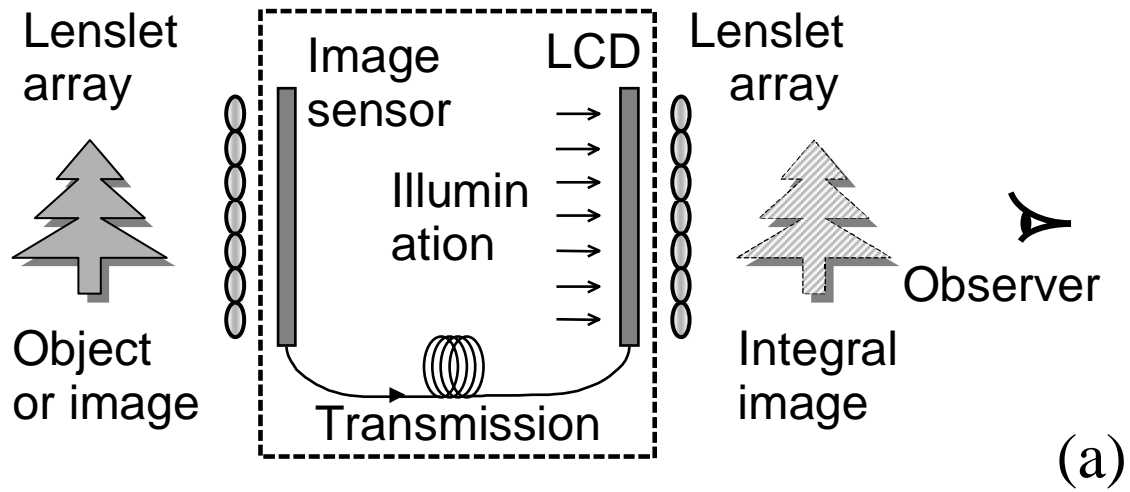


Fig. 3. (a) II system. (b) Experimental setup.

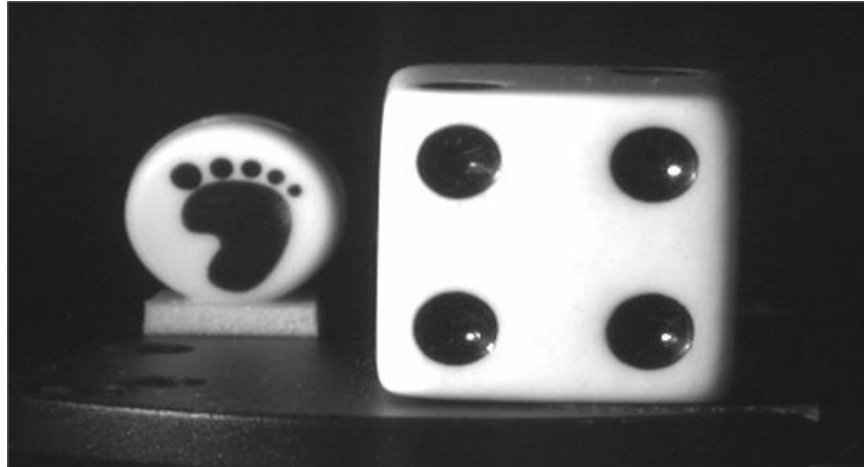


Fig. 4. Original object used for 3-D imaging experiments.

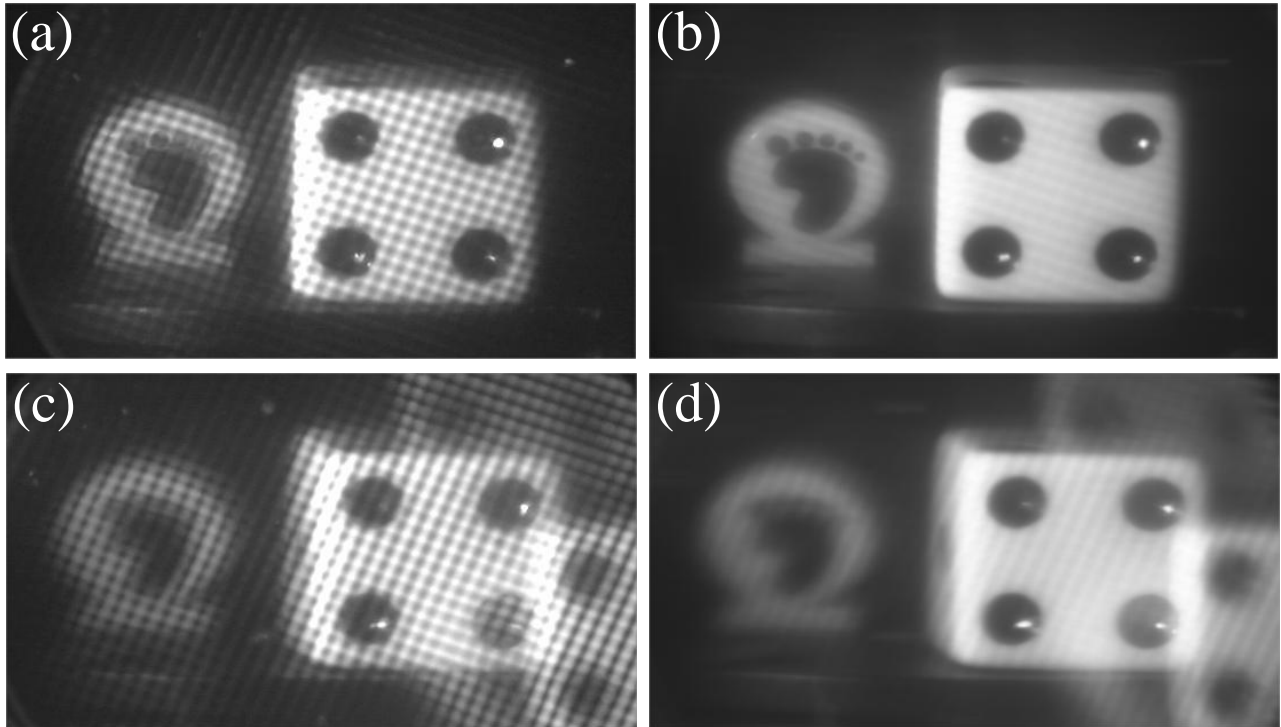


Fig. 5. (a) Experimental results for the 3-D image reconstruction. (b) On-axis observation. (c) and (d) Off-axis observation. In (b) and (d), the time-multiplexing technique was applied.

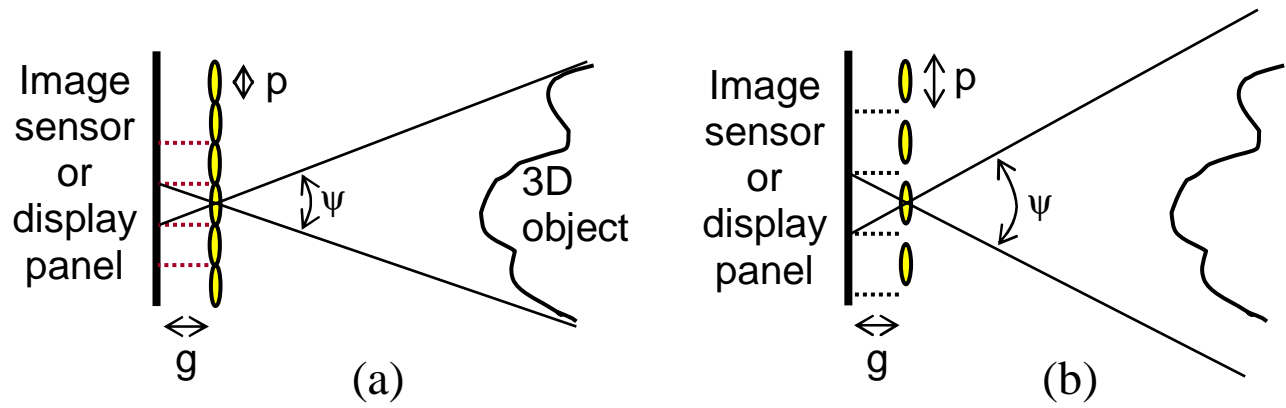


Fig. 6. Viewing angle and lenslet pitch. (a) Lenslet array with a high fill factor. (b) lenslet array with a low fill factor.

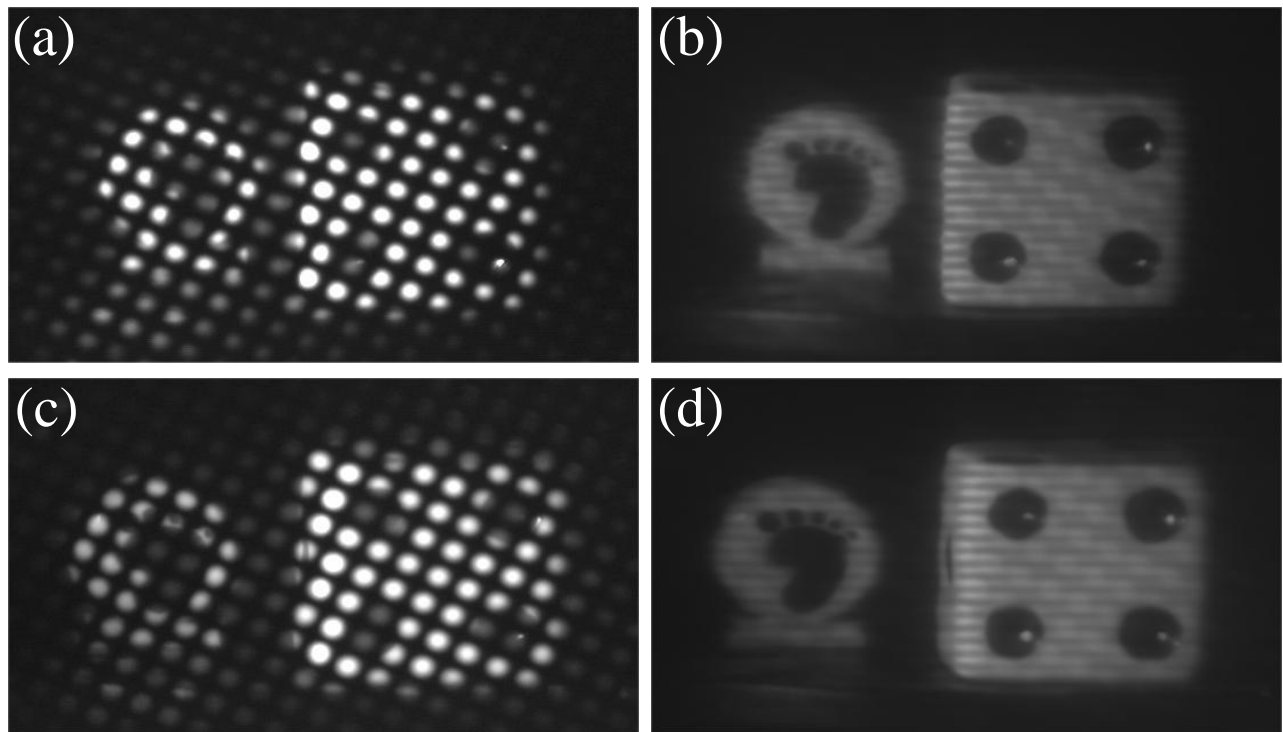


Fig. 7. (a) Experimental results for the 3-D image reconstruction using low fill-factor lenslet arrays. (b) On-axis observation. (c) and (d) Off-axis observation. In (b) and (d), the time-multiplexing technique was applied.

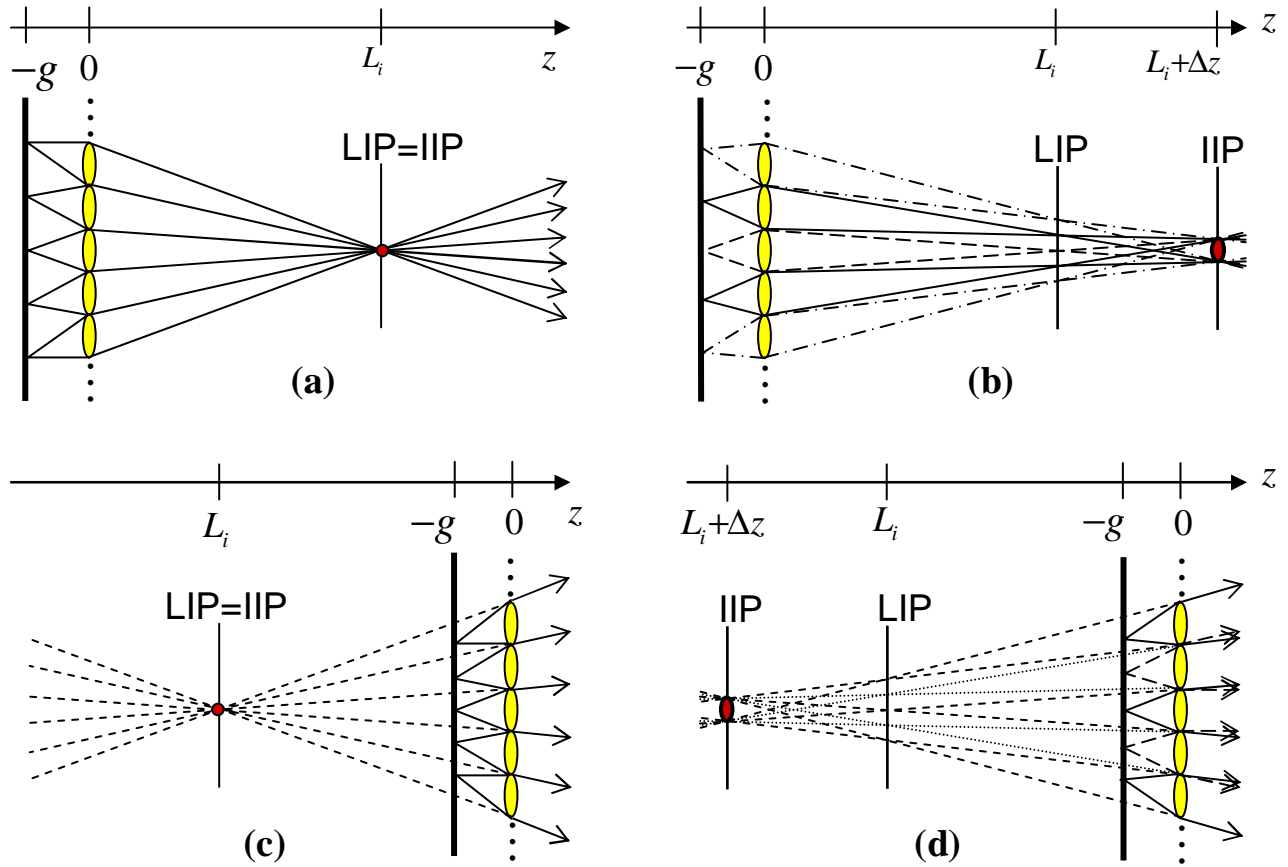


Fig. 8. (a) Ray integration to produce 3-D images in II. (b) Real image integration. (c) and (d) Virtual image integration. LIP: lenslet image plane; IIP: integral image plane.

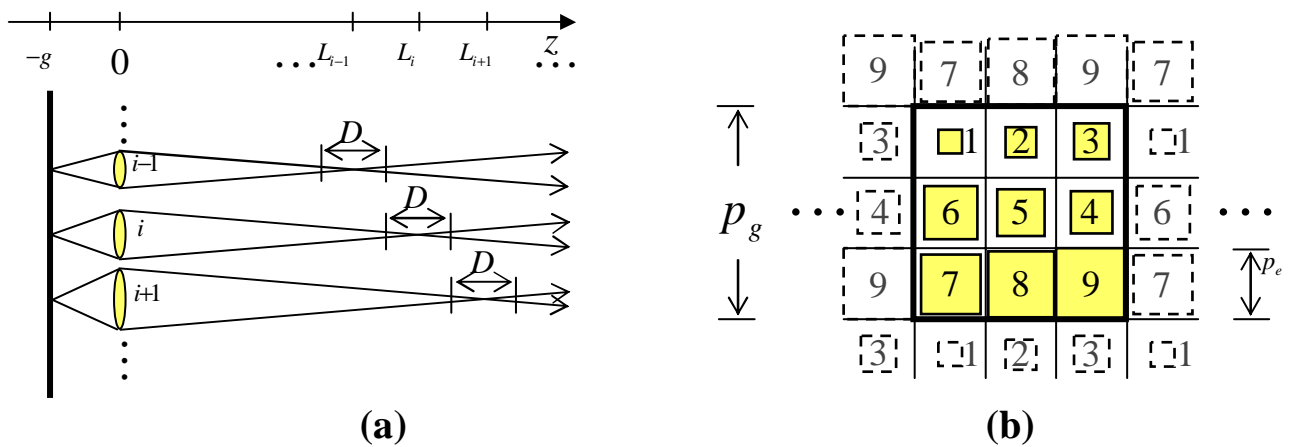


Fig. 9. The use of non-uniform lenslets. (a) The positions of lenslet image planes L_i when lenslets with different focal length and sizes are used. (b) Arrangement of different lenslets in the array.

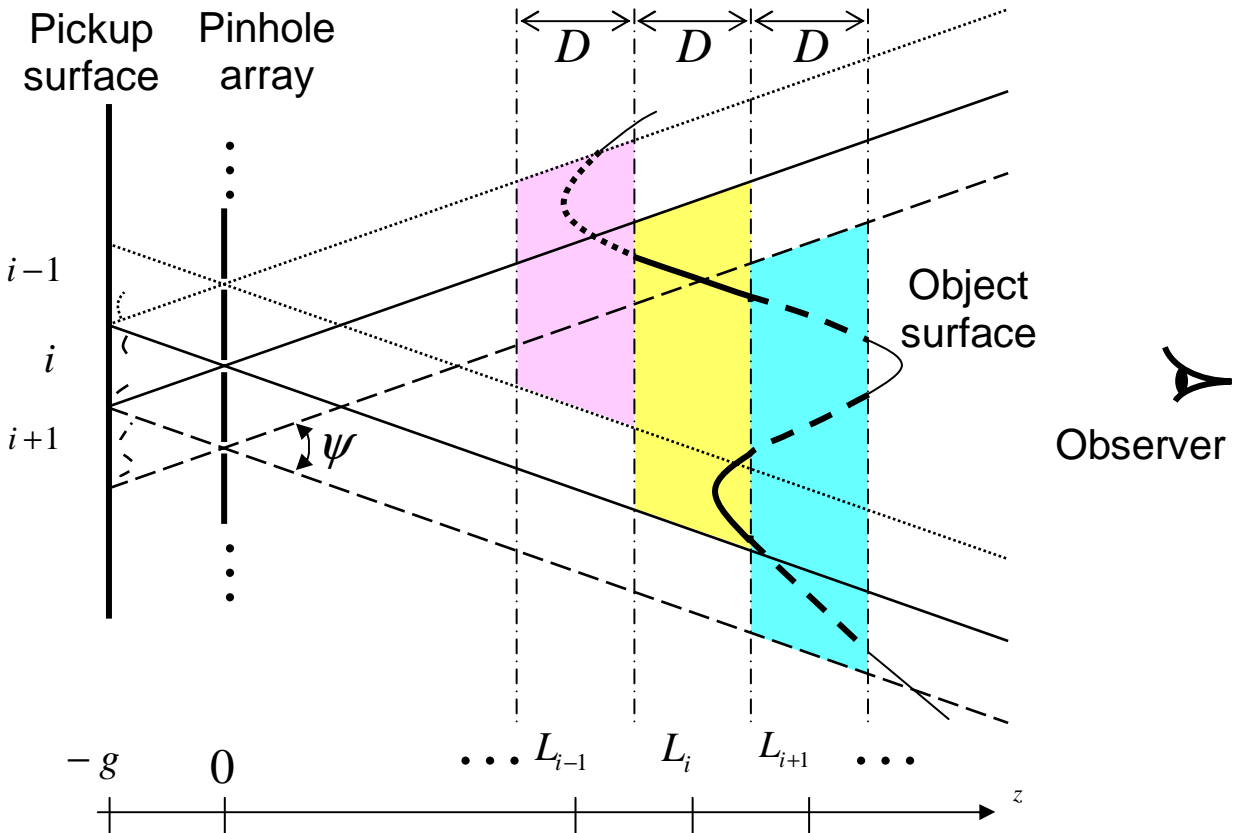


Fig. 10. Method to obtain elemental images by ray mapping. The object surfaces represented by the thick dotted line, the thick solid lines, and the thick dashed lines are mapped into the pickup surfaces corresponding to the $(i-1)$ th pinhole, the i th pinhole, and the $(i+1)$ th pinhole, respectively.